Competition between prismatic and basal slip in hexagonal titanium-aluminum alloys with short-range order

Piotr Kwasniak, Stéphanie Delannoy, Frédéric Prima, Emmanuel Clouet

Materials Research Letters

ISSN: (Print) (Online) Journal homepage: https://www.tandfonline.com/loi/tmrl20

Competition between prismatic and basal slip in hexagonal titanium–aluminum alloys with short-range order

P. Kwasniak, S. Delannoy, F. Prima & E. Clouet

To cite this article: P. Kwasniak, S. Delannoy, F. Prima & E. Clouet (2023) Competition between prismatic and basal slip in hexagonal titanium–aluminum alloys with short-range order, Materials Research Letters, 11:6, 407-413, DOI: 10.1080/21663831.2023.2169082

To link to this article: https://doi.org/10.1080/21663831.2023.2169082

Published online: 25 Jan 2023.

MATER. RES. LETT.
2023, VOL. 11, NO. 6, 407–413
https://doi.org/10.1080/21663831.2023.2169082

MATERIALS RESEARCH LETTERS
Taylor & Francis
Taylor & Francis Group

ORIGINAL REPORTS

Competition between prismatic and basal slip in hexagonal titanium–aluminum alloys with short-range order

P. Kwasniak[a], S. Delannoy[b], F. Prima[b] and E. Clouet[c]

[a]Multidisciplinary Research Center, Cardinal Stefan Wyszynski University in Warsaw, Warszawa, Poland; [b]Chimie ParisTech, CNRS, Institut de Recherche de Chimie Paris, PSL Research University, Paris, France; [c]Service de Recherches de Métallurgie Physique, Université Paris-Saclay, CEA, Gif-sur-Yvette, France

ABSTRACT

Plasticity of hexagonal titanium–aluminum alloys depends on the solute concentration and the order state of Al atoms. Development of short-range order (SRO) modifies Al strengthening and impacts the competition between prismatic and basal slip modes. Using *ab initio* calculations, we study the interaction of a screw dislocation with isolated Al atoms and Al pairs in an hcp Ti existing in short-range ordered Ti–Al alloys. Calculated activation energies reveal pronounced hardening caused by Al addition for both slip systems, which become competitive. This hardening is enhanced for Al pairs, resulting in a reduced plastic anisotropy of Ti–Al alloys with SRO.

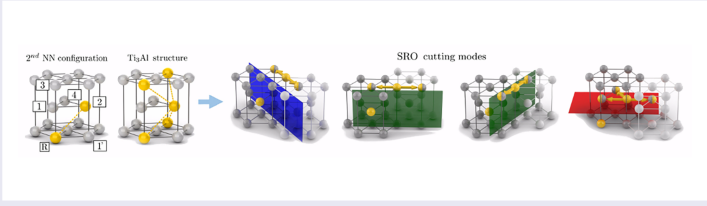

IMPACT STATEMENT

Short-range ordering is shown to impact plasticity in ahexagonal Ti–Al solid solution through *ab initio* modeling of dislocation interaction withsolute and pair of solute atoms.

ARTICLE HISTORY
Received 5 September 2022

KEYWORDS
Titanium–aluminum alloys; ordering; plasticity; dislocations

1. Introduction

Aluminum, the most widely used alloying element of titanium, exhibits pronounced tendency for ordering in hexagonal (α) Ti. Ordering occurs in α-Ti–Al alloys containing $\sim$ 6 wt.% or more Al and subjected to long-term heating at 500−800 °C. It leads not only to the formation of Ti_3Al clusters (α_2 phase) [1–8], which share the same underlying hexagonal lattice as the α phase, but also to short-range order (SRO) in the α solid solution, with the distribution of Al positions on the hexagonal lattice deviating from randomness. All such ordering phenomena, either presence of an α_2 second phase or the development of SRO in the α phase, substantially influence the mechanical properties of the material. Neeraj et al. [9,10] reported significant improvement of room temperature creep resistance of Ti–6Al alloy exhibiting order relative to disordered state. On the other hand, although nucleation of α_2, in general, increases the strength of the α-Ti–Al mixtures, [2,7,8,11–13] noticeable reduction in ductility, fatigue resistance and fracture toughness also takes place [7,8,12,14,15].

Formation of ordered domains induces a 'wavy to planar' slip transition, with the dislocation population switching from a homogeneous to a heterogeneous distribution, where planar arrangements of dislocations are formed [2,7–11,13,16–18]. Localization of plastic deformation in thin slip bands decreases the size of plastic deformation zones at the head of fatigue crack tips, leading to a reduction of ductility and fracture toughness [15]. Extensive experimental observations reveal that planar slip bands are preferentially localized on prismatic and basal planes with pairs of $1/3\langle 1\,\bar{2}\,1\,0\rangle$ screw dislocations on the head of the slip band [2,7,9,13,15,18]. Planar glide and dislocation pairing is attributed to antiphase boundary (APB), either perfect APB in the ordered α_2 compounds or diffuse APB in the α solid solution with SRO [3,19], formed at the onset of plastic deformation. APB corresponds to the destruction of the ordered state

CONTACT P. Kwasniak p.kwasniak@uksw.edu.pl

when the crystal is sheared by the slip of a dislocation, thus leading to an extra energy cost responsible for strengthening. Although slip by a second trailing dislocation partially restores the favorable distribution of alloying element, after a small number of slip events, the state of order is largely destroyed and subsequent dislocations experience negligible friction stress due to order [3]. In such a mechanism, dislocations located at the head or inside the slip bands experience different configurations of solutes (ordered and disordered, respectively). However, in both cases, line defects display the same corrugated form [7,9,13,18,20]. This specific shape of dislocation lines implies intensive cross slip. Recent experiments [7] confirm that slip is not fully planar at the atomic scale but delocalized on several adjacent planes.

These variations of mechanical properties stem from changes of active deformation modes in these titanium alloys. The main deformation mode in pure Ti is the glide of $\langle a \rangle$ dislocations with $1/3\langle 1\,\bar{2}\,1\,0\rangle$ Burgers vector in $\{1\,0\,\bar{1}\,0\}$ prismatic planes [17,21,22]. With an aluminum addition, the fraction of prismatic slip decreases in favor of slip in $(0\,0\,0\,1)$ basal planes, which is barely active in pure Ti [2,16,17,23,24]. Recent *ab initio* calculations show that the transition from prismatic to basal slip with the addition of simple metals like Al, In or Sn in titanium can be understood from the interaction of $1/3\langle 1\,\bar{2}\,1\,0\rangle$ screw dislocations with these solute atoms, which induce a similar energy barrier opposing dislocation glide on prismatic and basal planes [25–28]. These slip systems become then competitive with solute addition. Although solute elements like Al, In and Sn significantly reduce the energy of basal stacking fault, screw dislocations never dissociate in $(0\,0\,0\,1)$ basal planes but remain spread in prismatic and pyramidal planes [27,28]. As a consequence, simple calculations of interaction between stacking faults and solute atoms are inconclusive to understand the impact of solute addition on the competition between the different slip systems which needs to be addressed by a proper modeling of the dislocation core structure, considering the energy barrier when the dislocation glides in the vicinity of solute atoms.

Previous *ab initio* calculations did not consider any ordering effect, as they consider a screw dislocation interacting with a single solute atom. In this article, we extend this work to examine the influence of SRO on prismatic and basal slip in α-Ti–Al alloy. To this end, the structure, energy and Peierls energy barrier of $1/3\langle 1\,\bar{2}\,1\,0\rangle$ screw dislocations gliding along $\{1\,0\,\bar{1}\,0\}$ prismatic and $(0\,0\,0\,1)$ basal planes are determined, taking into account different configurations of solute atoms, which are representative of SRO existing in the solid solution. The purpose is to provide insight on the impact of SRO on the hardening of prismatic and basal slip systems and on their competition.

2. Methods

Density functional theory calculations were performed with the VASP code [29–31] and the full periodic boundary condition approach [32,33] was used to model screw dislocations. To minimize the solute interaction with its periodic images, a reasonably large 1152 atoms supercell with the quadrupolar arrangement of dislocations [34] was adopted. The simulation box periodicity vectors are $\vec{u}_1 = 9c\vec{e}_x$, $\vec{u}_2 = 4\sqrt{3}a\vec{e}_y$ and $\vec{u}_3 = 4a\vec{e}_z$, where a and c are the Ti lattice parameters and $\vec{e}_x, \vec{e}_y, \vec{e}_z$ are the unit cell vectors along $[0\,0\,0\,1]$, $[0\,1\,\bar{1}\,0]$ and $[\bar{2}\,1\,1\,0]$ directions, respectively [28]. The electronic structure of investigated systems was calculated using the projector augmented wave (PAW) method [35] and Perdew–Burke–Ernzerhof (PBE) [36] generalized gradient functional with a $1 \times 1 \times 3$ gamma-centered k-points grid and a 0.3 eV Methfessel–Paxton electronic occupancy smearing. The Ti ($3d^2 4s^2$) and Al ($3s^2 3p^1$) pseudopotentials and a 500 eV cutoff energy for plane waves were employed. Simulations of dislocation glide were conducted using the climbing image nudged elastic band (NEB) [37,38] method

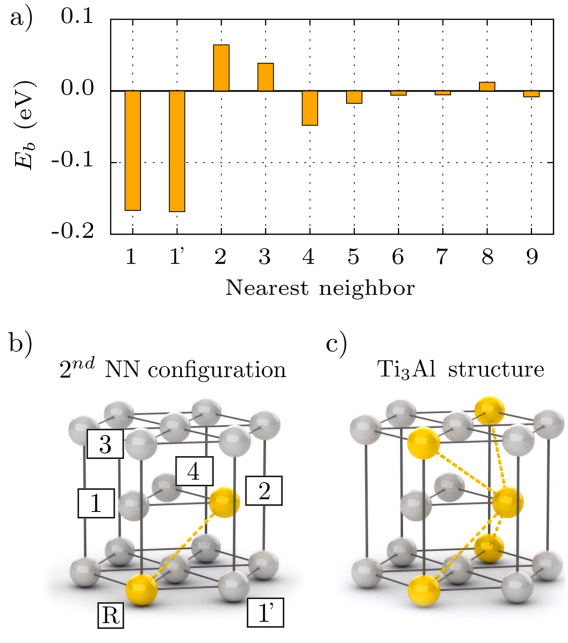

Figure 1. Binding energies E_b of Al pairs in α-Ti as a function of distance between solute atoms (a). Sketch of the hcp lattice indicating the five most strongly interacting NN configurations with the reference solute atom lying at R position (b). Crystal structure of the intermetallic Ti_3Al compound achieved by multiplication of the second and third NN Al pairs (c).

providing the minimum energy path between two stable configurations. Atomistic calculations were terminated after reaching a 3 and 25 meV/Å convergence criterion on Hellmann–Feynman forces for static relaxation and NEB calculations, respectively. The same computational setup with a 288 atoms simulation box ($5 \times 5 \times 4\alpha$-Ti unit cell periodicity along $[\bar{1}\,2\,\bar{1}\,0]$, $[2\,\bar{1}\,\bar{1}\,0]$ and $[0\,0\,0\,1]$ directions) and $3\times3\times3$ k-points mesh was used for calculations binding energy of Al pairs in α-Ti lattice.

3. Results and discussion

To verify the ordering tendency of Al atoms in α-Ti, the binding energies of Al pairs were calculated as a function of distance between solutes using the following definition:

$$E_b = 2E_{\mathrm{Ti+Al}} - E_{\mathrm{Ti}} - E_{\mathrm{Ti+2Al}}, \tag{1}$$

where E_{Ti}, $E_{\mathrm{Ti+Al}}$ and $E_{\mathrm{Ti+2Al}}$ are the total energy of the same supercell with pure Ti, the α-Ti structure alloyed with one isolated Al solute atom and with a pair of two solute atoms, respectively. Binding energies are calculated up to ninth nearest neighbor (NN), with one Al solute sitting at the position 'R' in Figure 1(b) and the second one at the numbered position 1, 2, …A positive binding energy E_b indicates attractive interaction between Al solutes for the pair of NN at given configuration. Binding energies for Al pairs (Figure 1(a)) show strong repulsion for the two first NN positions (configurations 1 and 1′) and attraction for the two next NN positions, i.e. the second and third NN positions. Interaction for the

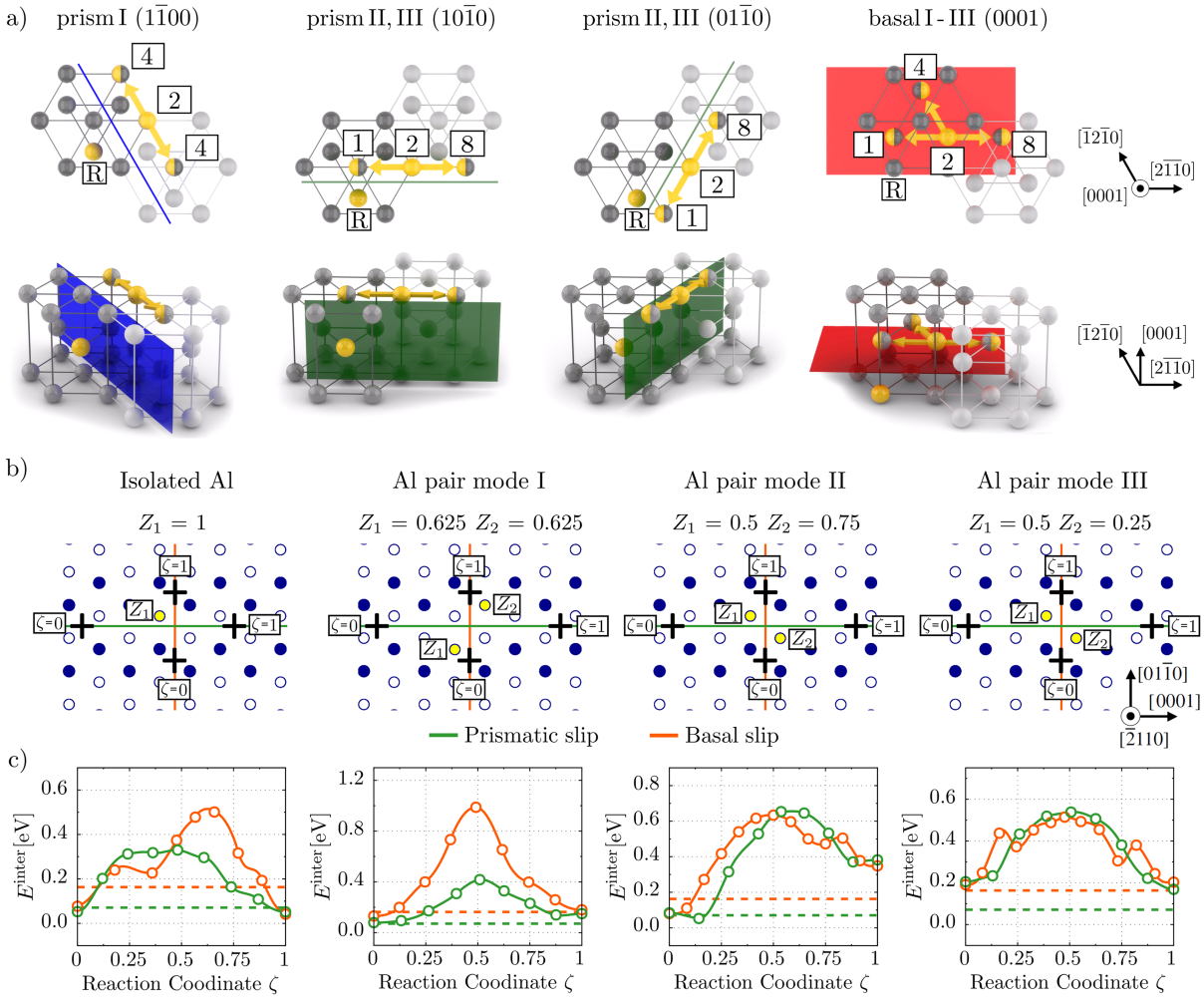

Figure 2. (a) Three geometrically possible prismatic and basal cutting modes of the second NN solute pair in α-Ti. (b) Initial $\zeta = 0$ and final $\zeta = 1$ positions of $1/3\langle 1\,\bar{2}\,1\,0\rangle$ screw dislocation gliding next to isolated Al atom or cutting the second NN Al pair along prismatic and basal modes I–III. Z_1 and Z_2 indicate the position (normalized by the lattice parameter a) of solute atoms along dislocation line in the simulation box. Ti atoms belonging to different $(\bar{2}\,1\,1\,0)$ are plotted with open or full-colored circles. Solute atoms are denoted by yellow color. The corresponding minimum energy paths of particular prismatic and basal slip modes are given in (c), with the Peierls energy barriers of pure Ti marked by dashed lines.

more distant configurations is either slightly repulsive or almost null. Ordering in Ti–Al alloys should therefore promote the formation of the second and third NN pairs. Multiplication of these energetically favorable states leads to the crystal structure of the ordered Ti_3Al compound (Figure 1(c)) indicating that these NN Al pairs are the elementary ordered units of the experimentally detected α_2 phase [1,4,5]. SRO in the solid solution will lead to an enhanced probability for such pairs because of their attractive binding energy and gliding dislocations will interact not only with isolated Al solute atoms but also with pairs of the second and third NN in solid solution which have been aged to promote SRO. *Ab initio* calculations of the interaction between dislocations and these pairs of solute atoms offer thus a natural way to understand how SRO in the Ti–Al solid solution may impact plasticity in the α phase.

As described in the previous section, plastic deformation of the solid solution in the presence of SRO destroys the favorable distribution of solute atoms. Taking into account pronounced variations of the solute binding energy E_b (Figure 1(a)), it is expected that the energy barrier of dislocation glide in such a scenario depends on the geometry of SRO cutting mode, i.e. crystallographic relation between slip plane and solute pair corresponding to SRO defining change of the relative position of solutes after dislocation glide. For the pair of the second NN corresponding to the strongest solute attraction, three SRO cutting modes for prismatic and basal slip can be distinguished, as presented in Figure 2(a). The corresponding reconfigurations of ordered solutes are as follow: second → fourth NN (mode I), second → first NN (mode II), and second → eighth NN (mode III). These are the only three possible cutting modes for this second NN pair, corresponding to the three possible $1/3\langle 1\,\bar{2}\,1\,0\rangle$ Burgers vectors. SRO cutting modes of the third NN will not be considered, as this configuration is less attractive than the second NN pair, and its shear leads to less repulsive interaction.

To reveal the influence of SRO on competition between prismatic and basal slip, glide of the $1/3\langle 1\,\bar{2}\,1\,0\rangle$ screw dislocation through the second NN in all three cutting modes has been modeled and compared to equivalent deformation for a dislocation interacting with an isolated solute atom in the same supercell, and thus for the same 4b dislocation length (Figure 2(b)). These second NN Al pairs and isolated solute atoms correspond to the different main obstacles encountered by a gliding dislocation in a Ti–Al solid solution with and without SRO. E^{act} of gliding dislocation is defined as the maximum of the interaction energy E^{inter} between the gliding dislocation and solutes, with

$$E^{\mathrm{inter}} = \frac{1}{2}(E_{tot} - E_{\pi l} - E_{sol} + E_{Ti}), \tag{2}$$

Table 1. Activation energies E^{act} and its difference ΔE^{act} relative to pure Ti for a $\langle a\rangle$ screw dislocation gliding in prismatic and basal planes in pure Ti and Ti–Al systems with distinct configurations of solute atoms. Activation energies are given in meV and are calculated for a single dislocation of length (Figure 2(b)).

Solutes configuration	Slip mode	E^{act}	ΔE^{act}
Pure Ti	Prism	71	0
	Basal	163	0
Ti + isolated Al	Prism	330	259
	Basal	501	338
Ti + Al SRO	Prism I	417	346
	Basal I	988	825
	Prism II	654	583
	Basal II	634	471
	Prism III	538	467
	Basal III	514	351

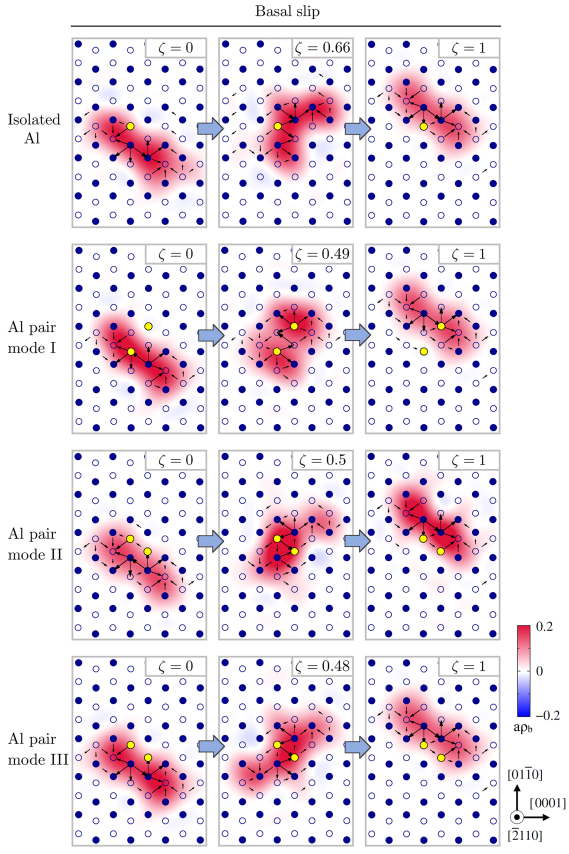

Figure 3. Core structure of the $\langle a\rangle$ screw dislocation gliding on basal plane along isolated Al atom or cutting the second NNN Al pairs with I–III cutting modes. Selected states are the initial, maximum energy and final configuration of each glide mode from Figure 3. The arrows between atomic columns are proportional to the differential displacement created by the dislocation in the $[\bar{2}\,1\,1\,0]$ direction. Displacement smaller than $0.1b$ is not shown. The contour map shows the dislocation density according to the Nye tensor.

where E_{tot}, $E_{\pi l}$, E_{sol} and E_{Ti} are the total energy of the same supercell which contains respectively a dislocation dipole with the particular solutes distribution on each dislocation, the dipole in pure Ti with the dislocations in their ground state pyramidal configuration, equivalent position of solutes without line defects and perfect pure Ti structure. The variations of the interaction energy along the minimum energy paths calculated with the NEB method [38] are plotted in Figure 2(c). Corresponding activation energies are listed in Table 1.

Obtained activation energies strongly depend on the orientation of the Al pair and on the dislocation glide plane. For prismatic slip, mode II leads to the highest activation energy, while the highest energy is obtained with mode I for basal slip. Interestingly, mode II and mode III lead to almost the same activation energy for prismatic and basal slip, while the activation energy still remains higher for basal than for prismatic slip in mode I. Pairs of solute atoms arising from SRO should reduce the plastic anisotropy, with prismatic slip becoming almost as hard as basal slip in the presence of Al pairs. The same conclusion was reached from the interaction of screw dislocation with isolated simple metals [28], but the reduction of plastic anisotropy through a decrease of the difference of activation energies appears more marked for Al pairs than for isolated Al atoms (Table 1). This offers a possible explanation to experiments reporting an increase of basal slip activity in α Ti–Al alloys in the presence of chemical ordering [2,9,15,16,23].

The contribution to hardening of the different solute configurations may be also discussed by looking to the variation ΔE^{act} of activation energy compared to pure Ti. For prismatic slip, pairs of solute atoms lead to larger energy barriers than isolated atoms for all slip modes. One therefore expects stronger hardening of the prismatic slip system in the presence of SRO than in the fully disordered state: although agglomeration of Al atoms in pairs reduces, for a fixed nominal concentration, the density of obstacles, each obstacle is a stronger obstacle. Things are not as clear for basal slip as the pair of solute atoms corresponding to mode III leads to the same variation of the activation energy as an isolated Al atom. Such a pair is not a stronger obstacle than an isolated Al atom. Development of SRO could therefore lead to a softening of basal slip.

To clarify the substantially different E^{act} obtained for isolated Al and pairs of solute atoms corresponding to different SRO cutting modes, the structures of $1/3\langle 1\,\bar{2}\,1\,0\rangle$ screw dislocation gliding on basal and prismatic planes are shown in Figures 3 and 4. In the case of basal slip, the highest states along the minimum energy paths exhibit important spreading in the basal plane while still remaining partially spread also on prismatic and pyramidal planes. This is a consequence of the attractive interaction between Al atoms and the basal stacking fault [25], leading to a pinning of the fault ribbon in the basal plane as already modeled in Ti+Sn and Ti+In alloys [28]. Formation of basal stacking faults (SF) is expected as it is

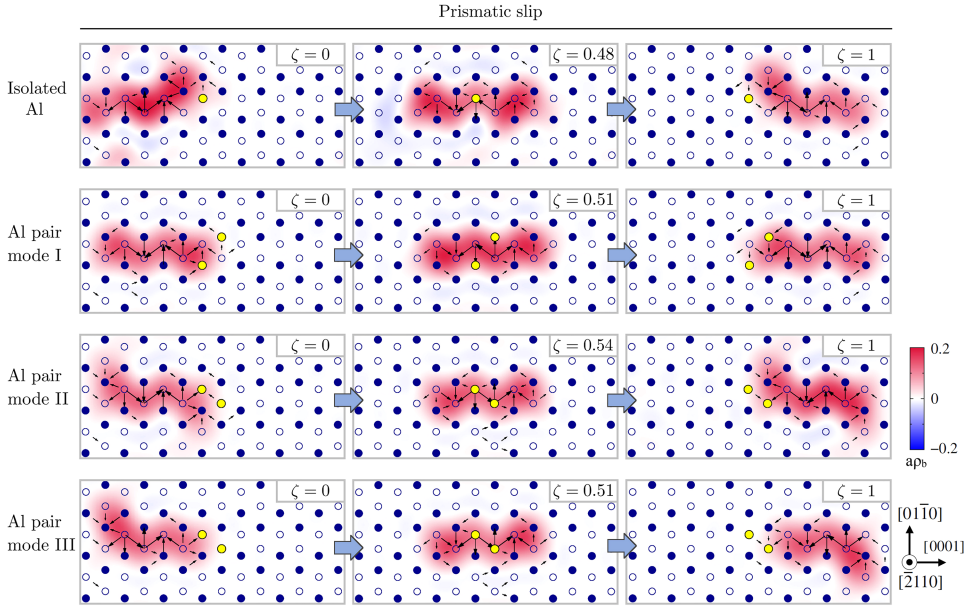

Figure 4. Core structure of the $\langle a\rangle$ screw dislocation gliding on prismatic plane along isolated Al atom or cutting the second NNN Al pairs with I–III cutting modes. Selected states are the initial, maximum energy and final configuration of each glide mode from Figure 3. The arrows between two atomic columns are proportional to the differential displacement created by the dislocation in the $[\bar{2}\,1\,1\,0]$ direction. Displacement smaller than $0.1b$ is not shown. The contour map shows the dislocation density according to the Nye tensor.

known that simple metals efficiently reduce the energy of this configuration in α-Ti [25]. Since for the different SRO cutting modes the Al atoms are differently oriented relative to slip plane, distance between solutes at particular crystallographic direction also varies. According to Figure 3, distance between Al atoms along $[0\,1\,\bar{1}\,0]$ in mode I is $2a\sqrt{3}/3$ while in modes II and III is $a\sqrt{3}/3$ (a is the lattice parameter of α-Ti). For such configurations, the basal SF ribbon is larger in mode I than in modes II and III, thus leading to a higher energy cost, in agreement with the activation energy barriers.

On the other hand, prismatic slip is executed with a planar prismatic structure of $1/3\langle 1\,\bar{2}\,1\,0\rangle$ screw dislocation (Figure 4) without additional significant core dissociation in any modes which justifies a smaller energy variation of this deformation path. Here the distance between solutes along $[0\,0\,0\,1]$ in $(0\,1\,\bar{1}\,0)$ glide plane is equal, however, Al atoms are located in the first nearest prismatic planes above and below the glide plane in modes II and III which according to previous calculations [25] most strongly increases the energy of prismatic SF. As a result, cutting modes II and III have a higher activation energy of prismatic slip than mode I (Table 1).

4. Summary and conclusions

In summary, the chemical ordering of Al in α-Ti displays a strong impact on the behavior of $1/3\langle 1\,1\,\bar{2}\,0\rangle$ screw dislocations gliding on prismatic and basal planes. This atomic-scale effect is related with the new crystallographic parameters of plasticity, i.e. the SRO cutting modes which specify reconfiguration of favorably distributed solute atoms upon the single slip event. The investigated solute clusters corresponding to SRO in the solid solution are formed from the elementary second NN Al pairs and undergo transition to fourth, first or eighth NN positions in cutting modes I, II and III, respectively. Since the binding energy of Al atoms on these sites varies with the amplitude of 231 meV, particular cutting modes contribute differently to strengthening. The increase in activation energy of dislocation glide is highly non-uniform, e.g. 2.4 times larger in basal mode I than in basal mode III. We found that this strengthening inhomogeneity arises also from two interrelated factors: (i) dissimilar reconfiguration of line defects and (ii) interaction of solute atoms with the stacking fault appearing in the dislocation cores. Finally, the comparison of activation energies of prismatic and basal slip indicates that isolated Al atoms provide pronounced hardening of both deformation modes. SRO significantly enhances this effect leading to the same activation energy of prismatic and basal glide in modes II and III. Obtained energy barriers for the different obstacles, isolated solute atoms and NN pairs appearing with SRO, are the quantities needed by solid solution strengthening theories [39]. As a perspective, it will be possible to model how hardening varies with the temperature and the ordering state of the solid solution for a given Al nominal concentration.

Acknowledgments

The authors acknowledge the PL-GRID infrastructure, which provided the computational resources—the Promethus and Tryton supercomputers.

Data availability

All data needed to evaluate the conclusions in the paper are present in the paper and/or the Supplementary Materials. Any additional details are available from the corresponding author upon reasonable request.

Disclosure statement

No potential conflict of interest was reported by the authors.

Funding

This work was financially supported by the Polish National Science Centre under grant no. 2019/35/D/ST5/02379 (UMO-2019/35/D/ST5/02379) and Polish Ministry of Education within the grant no. MEiN/2022/DPI/1064.

References

[1] Namboodhiri TKG, McMahon CJ, Herman H. Decomposition of the α-phase in titanium-rich Ti–Al alloys. Metall Mater Trans B. 1973;4(5):1323–1331.
[2] Williams JC, Baggerly RG, Paton NE. Deformation behavior of HCP Ti–Al alloy single crystals. Metall Mater Trans A. 2002;33(3):837–850.
[3] van de Walle A, Asta M. First-principles investigation of perfect and diffuse antiphase boundaries in HCP-based Ti–Al alloys. Metall Mater Trans A. 2002;33(3):735–741.
[4] Radecka A, Bagot PAJ, Martin TL, et al. The formation of ordered clusters in Ti–7Al and Ti–6Al–4V. Acta Mater. 2016;112:141–149.
[5] Gardner HM, Radecka A, Rugg D, et al. A study of the interaction of oxygen with the $\alpha 2$ phase in the model alloy Ti–7wt%Al. Scr Mater. 2020;185:111–116.
[6] Dear FF, Kontis P, Gault B, et al. Mechanisms of Ti3Al precipitation in hcp α-Ti. Acta Mater. 2021;212:Article ID 116811.
[7] Zhang R, Zhao S, Ophus C, et al. Direct imaging of short-range order and its impact on deformation in Ti-6Al. Sci Adv. 2019;5(12):eaax2799.
[8] Chong Y, Zhang R, Hooshmand MS, et al. Elimination of oxygen sensitivity in α-titanium by substitutional alloying with Al. Nat Commun. 2021;12(6158):1–9.
[9] Neeraj T, Hou DH, Daehn GS, et al. Phenomenological and microstructural analysis of room temperature creep in titanium alloys. Acta Mater. 2000;48(6):1225–1238.

[10] Neeraj T, Mills MJ. Short-range order (SRO) and its effect on the primary creep behavior of a Ti–6wt.%Al alloy. Mater Sci Eng A. 2001;319–321:415–419.
[11] Truax DJ, McMahon CJ. Plastic behavior of titanium–aluminum alloys. Mater Sci Eng. 1974;13(2):125–139.
[12] Wu Z, Qiu C, Venkatesh V, et al. The influence of precipitation of alpha2 on properties and microstructure in TIMETAL 6-4. Metall Mater Trans A. 2013;44(4):1706–1713.
[13] Castany P, Pettinari-Sturmel F, Douin J, et al. TEM quantitative characterization of short-range order and its effects on the deformation micromechanims in a Ti–6Al–4V alloy. Mater Sci Eng A. 2017;680:85–91.
[14] Zhang XD, Evans DJ, Baeslack WA, et al. Effect of long term aging on the microstructural stability and mechanical properties of Ti–6Al–2Cr–2Mo–2Sn–2Zr alloy. Mater Sci Eng A. 2003;344(1):300–311.
[15] Youssef SS, Zheng X, Huang S, et al. Precipitation behavior of $\alpha 2$ phase and its influence on mechanical properties of binary Ti–8Al alloy. J Alloys Compd. 2021;871:Article ID 159577.
[16] Sakai T, Fine ME. Plastic deformation of Ti–Al single crystals in prismatic slip. Acta Metall. 1974 Nov;22(11):1359–1372.
[17] Caillard D, Gaumé M, Onimus F. Glide and cross-slip of a-dislocations in Zr and Ti. Acta Mater. 2018 Aug;155:23–34.
[18] Radecka A, Coakley J, Jones IP, et al. Ordering and the micromechanics of Ti–7Al. Mater Sci Eng A. 2016 Jan;650:28–37.
[19] Fisher JC. On the strength of solid solution alloys. Acta Metall. 1954;2(1):9–10.
[20] Zhao S, Zhang R, Chong Y, et al. Defect reconfiguration in a Ti–Al alloy via electroplasticity. Nat Mater. 2021 Apr;20(4):468–472.
[21] Farenc S, Caillard D, Couret A. An in situ study of prismatic glide in α titanium at low temperatures. Acta Metall Mater. 1993;41(9):2701–2709.
[22] Clouet E, Caillard D, Chaari N, et al. Dislocation locking versus easy glide in titanium and zirconium. Nat Mater. 2015;14(9):931–936.
[23] Sakai T, Fine ME. Basal slip of xn–TiAl-c13v single crystals. Scr Metall. 1974 May;8(5):545–547.
[24] Zaefferer S. A study of active deformation systems in titanium alloys: dependence on alloy composition and correlation with deformation texture. Mater Sci Eng A. 2003 Mar;344(1):20–30.
[25] Kwasniak P, Garbacz H, Kurzydlowski KJ. Solid solution strengthening of hexagonal titanium alloys: restoring forces and stacking faults calculated from first principles. Acta Mater. 2016 Jan;102:304–314.
[26] Kwasniak P, Garbacz H. Screw dislocation mediated solution strengthening of substitutional α-Ti alloys – first principles investigation. Acta Mater. 2017 Dec;141:405–418.
[27] Kwasniak P, Clouet E. Basal slip of ⟨a⟩ screw dislocations in hexagonal titanium. Scr Mater. 2019;162:296–299.
[28] Kwasniak P, Clouet E. Influence of simple metals on the stability of ⟨a⟩ basal screw dislocations in hexagonal titanium alloys. Acta Mater. 2019;180:42–50.
[29] Kresse G, Hafner J. Ab initio molecular dynamics for liquid metals. Phys Rev B. 1993;47(1):558–561(R).
[30] Kresse G, Furthmüller J. Efficiency of ab-initio total energy calculations for metals and semiconductors using a plane-wave basis set. Comput Mater Sci. 1996;6(1):15–50.
[31] Vienna Ab initio Simulation Package. Available from: https://www.vasp.at.
[32] Rodney D, Ventelon L, Clouet E, et al. Ab initio modeling of dislocation core properties in metals and semiconductors. Acta Mater. 2017;124:633–659.
[33] Clouet E. Ab initio models of dislocations. In: Andreoni W, Yip S, editors. Handbook of materials modeling. Springer International Publishing; 2018. p. 1–22.
[34] Clouet E, Ventelon L, Willaime F. Dislocation core energies and core fields from first principles. Phys Rev Lett. 2009 Feb;102(5):Article ID 055502.
[35] Blöchl PE. Projector augmented-wave method. Phys Rev B. 1994;50:17953–17979.
[36] Perdew JP, Burke K, Ernzerhof M. Generalized gradient approximation made simple. Phys Rev Lett. 1996;77:3865–3868.
[37] Henkelman G, Uberuaga BP, Jónsson H. A climbing image nudged elastic band method for finding saddle points and minimum energy paths. J Chem Phys. 2000;113(22):9901–9904.
[38] Sheppard D, Terrell R, Henkelman G. Optimization methods for finding minimum energy paths. J Chem Phys. 2008;128(13):Article ID 134106.
[39] Varvenne C, Leyson GPM, Ghazisaeidi M, et al. Solute strengthening in random alloys. Acta Mater. 2017 Feb;124:660–683.